JACS
JOURNAL OF THE AMERICAN CHEMICAL SOCIETY
Article
Cite This: J. Am. Chem. Soc. 2018, 140, 5764−5773
pubs.acs.org/JACS

Concurrent Cooperative J-Aggregates and Anticooperative H-Aggregates

Kang Cai,[†,§] Jiajun Xie,[†,§] Di Zhang,[†] Wenjing Shi,[†] Qifan Yan,*[,‡] and Dahui Zhao*[,†]

[†]Beijing National Laboratory for Molecular Sciences, Centre for Soft Matter Science and Engineering, Key Lab of Polymer Chemistry & Physics of the Ministry of Education, College of Chemistry, Peking University, Beijing 100871, China

[‡]Key Laboratory for Advanced Materials, School of Chemistry and Molecular Engineering, East China University of Science and Technology, Shanghai 200237, China

Supporting Information

ABSTRACT: Completely understanding the working mechanisms of sophisticated supramolecular self-assembly exhibiting competing paths is very important for chemists en route to acquiring the ability of constructing supramolecular systems with controlled structures and designed functions. Here, the self-aggregation behaviors of an N-heterocyclic aromatic dicarboximide molecule **1**, boasting two competing paths that give rise to different supramolecular structures and exhibit distinct thermodynamic features, are carefully examined. First, a group of H-aggregates are observed when providing a medium driving force for aromatic stacking, and their formation is manifested as an anticooperative process. When exposed to enhanced strength of aromatic interactions, these H-aggregates are found to transform into J-aggregates via a cooperative assembly mechanism. With the assistance of a mathematic model accommodating two competing polymerization pathways, calculations are conducted to simulate and explain the thermodynamic equilibria of such a unique supramolecular system. The calculation results are highly consistent with the experimental observations, and some important properties are elucidated. Specifically, the anticooperative assembly mechanism generally promotes the formation of low to medium oligomers, whereas the cooperative path is more competent at producing high polymers. If the anticooperative and cooperative routes coexist and compete for the same molecule, the cooperative formations of high polymers are significantly suppressed unless a very high degree of polymerization can be achieved. Such a unique feature of concurring anticooperative and cooperative paths emerges to the H- and J-aggregates of molecule **1** and thus brings about the interesting sequential appearances of the two types of aggregates under conditions of continuously enlarged driving force for self-aggregation. Finally, based on the knowledge acquired from this study and by analyzing the steric features of **1** that influence its supramolecular packing motifs, a slightly modified molecular structure is designed, with which the intermediate H-aggregation state was successfully suppressed, and a single cooperative J-aggregation path is manifested.

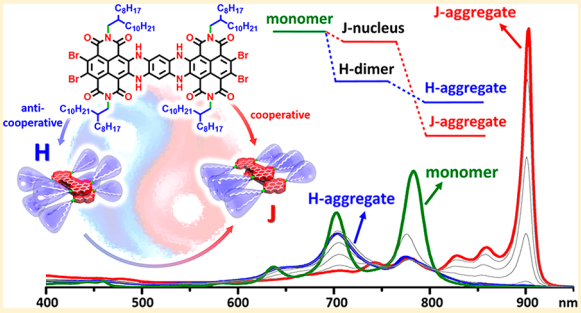

INTRODUCTION

The supramolecular structures of π-conjugated molecules are very important because they sensitively influence the performance of organic optoelectronic and semiconducting materials in both crystalline and solution-processed thin-film states.[1−3] H- and J-aggregates are the representative examples demonstrating that distinct supramolecular structures give rise to disparate optical and electronic properties. The blue-shifted absorption band exhibiting a lower 0−0/0−1 vibronic peak ratio than the value shown by the monomer is indicative of H-aggregate formation, and the fluorescence emission quenching is typically observed due to the vanished oscillator strength at the bottom of the excitonic band formed by face-to-face stacked (aggregated) molecules.[4] This forbidden nature of the lowest excited state is also conducive to the electron transfer process, and the cofacial molecular arrangements are generally favorable for charge carrier transport with semiconductors.[5] In contrast, red-shifted absorption with narrowed bandwidth and enhanced 0−0/0−1 ratio compared to the monomer are the symbolic features of J-aggregates. Amplified emission with accelerated decay rate may also be observed by virtue of the enlarged oscillator strength of the lowest excited state. These unique photophysical properties are of special value to energy transport and light-emitting functions,[6] and they are known to result from the coherent coupling of the transition moments of aggregated molecules. For the coherent coupling to occur, the molecules necessarily assume large lateral offsets along their transition dipoles in the aggregated state.[4] More recent studies have shown that, in addition to the Coulomb coupling, the short-range interactions arising from wave function overlap between the closely spaced neighboring molecules can also induce the transformation between H- and J-aggregates.[7] Evidently, the distinct properties of H- and J-aggregates render

Received: February 6, 2018
Published: April 12, 2018

DOI: 10.1021/jacs.8b01463
J. Am. Chem. Soc. 2018, 140, 5764−5773

them suitable for different functions and applications. However, although the correlation between these supramolecular structures and their respective optical features is generally explainable with the exciton coupling theories, the ability to precisely control and fine-tune the supramolecular structures is yet to be acquired by researchers. This is because the supramolecular behaviors of organic molecules are dictated by a collection of different noncovalent interactions, which show intricate dependences on the electronic and steric features of chemical structures. In order to gain more insightful understanding about the underlying principles that govern the supramolecular structure formation, extensive studies have been carried out with various H- and J-aggregate systems. The ultimate goal is to obtain molecular materials with predictable properties through rational design of their chemical structures.[8,9]

Among the various molecular aggregates investigated, sophisticated behaviors were observed. For example, dual H- and J-aggregate motifs were exhibited by the same molecule, or completely different (H- and J-) aggregate features were adopted by very similar molecular structures.[10] We deem that these unique systems deserve special attention because they offer vital clues to the key factors that govern the competition process and outcome of H- and J-aggregations. As unveiling a clear correlation between the chemical and supramolecular structures is the crucial step toward the aggregate structure control and property prediction, we herein conduct an in-depth study on the self-aggregation of a polycyclic aromatic molecule **1** (Chart 1), which uniquely manifests interesting concurrent

Chart 1. Chemical Structures of Molecules 1 and 2[a]

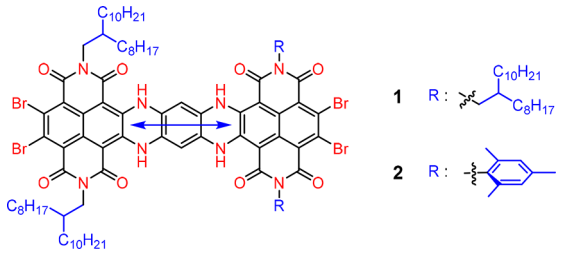

[a]The arrow indicates the direction of DFT-calculated S_0–S_1 transition dipole.

and competing H- and J-aggregation pathways. It is found that, in addition to the chemical structures, the energetic features of the assembling pathways play an important role in determining the competition outcome of different (e.g., H- vs J-) aggregation motifs.

In the literature, three different mechanistic models are applicable to describe the energetic characteristics of supramolecular polymerizations.[11] The isodesmic model, also known as the equal-*K* model, presents a simple situation where the association constants (K) remain constant for all association steps taking place between monomers, oligomers, and polymers, regardless of their sizes.[12] The cooperative mechanism corresponds to a polymerization that depicts an energy less favored oligomerization stage, and once the growing species reach a critical size, subsequent polymerization becomes much more favored in energy. Such a cooperative process is also named nucleation–elongation (N–E) polymerization.[13] In contrast, an anticooperative system refers to a polymerization in which the formations of low oligomers are more favored in energy compared to the high polymers, or the association constant may attenuate with the increasing size of polymers.[14]

To illustrate the effect of cooperative and anticooperative mechanisms, a qualitative comparison of the thermodynamic product distribution among the three types of polymerization systems is shown in Figure 1. Theoretical studies have shown

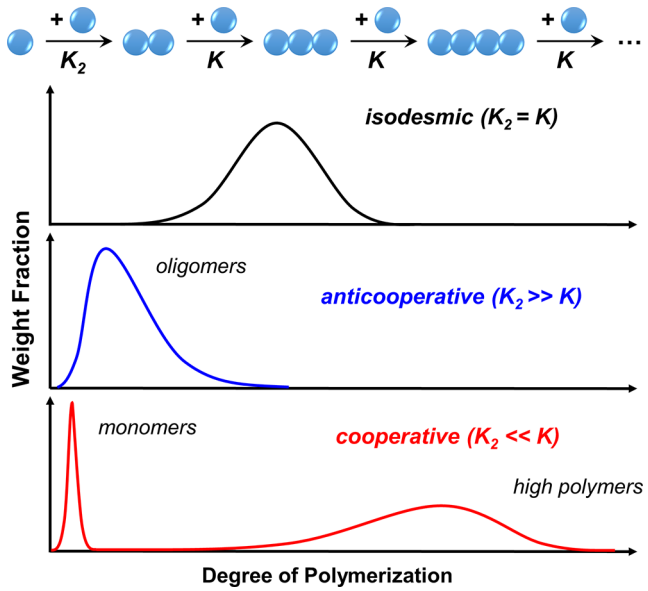

Figure 1. Schematic illustration and qualitative comparison of product size distributions in isodesmic, cooperative, and anticooperative polymerization systems with a similar association constant *K*.

that more pronounced differences can be observed when the variation of association constant occurs only for the very first few steps of polymerization.[13,14] Hence, when conducting the simulations, the dimerization constant (K_2) is set to be different from all the following chain growth steps, which are defined with an identical association constant (K). The calculation results (see SI for details) clearly demonstrate that, when K_2 is larger than K (i.e., an anticooperative mechanism), the average degree of polymerization is lowered compared to that of an equal-K system. In contrast, if $K_2 < K$ (cooperative path), a bimodal distribution emerges, with a set of high polymers formed coexisting with a significant number of free monomers.[11,15] The average degree of polymerization at the equilibrium (with unreacted monomer excluded) can be higher than those attained from an isodesmic and anticooperative polymerization with the same K (Figure S9).[12,13] Boasting such unique capability of generating high polymers, the cooperative mechanism attracts a great deal of attention. Although the N–E mechanism is widely observed with a range of biopolymers, including some proteins,[16] a rational design of synthetic (supramolecular) polymers exhibiting a cooperative chain growth process remains challenging. Hence, it is highly desirable to identify the general (supramolecular) structural features that effectively induce the N–E growth mechanism favoring high polymers.

Previously, we showed that the J-aggregate formation was successfully promoted with carefully designed molecule **1**, by installing a suitable number of side chains with tailored steric hindrance at appropriate positions around its planar polycyclic aromatic skeleton to obstruct the largely face-to-face and twisted stacking motifs.[17] Interestingly, in the current work

DOI: 10.1021/jacs.8b01463
J. Am. Chem. Soc. 2018, 140, 5764–5773

more detailed studies show that molecule **1** actually exhibits dual assembly motifs (i.e., low H-oligomers and high J-aggregates). Moreover, the two aggregation pathways display contrasting anticooperative and cooperative assembly mechanisms. By carrying out temperature- and solvent-dependent studies, the H-aggregates are found to exist only in the intermediate temperature range and in solvents of medium polarity. They are transformed into J-aggregates when exposed to an enhanced driving force of intermolecular aggregation. Furthermore, taking advantage of their disparate absorption properties and examining their respective temperature and concentration dependencies, we are able to disentangle the respective energetic features of J- and H-assemblies. The formation of an H-aggregate presents an anticooperative characteristic, whereas the J-aggregate features a cooperative assembling mechanism. Next, by setting up a pertinent mechanistic model, the thermodynamic properties of such dual-aggregation-path supramolecular system are simulated and investigated in detail. The calculation results reveal that the different energetics (anticooperative vs cooperative) of the two types of aggregates are crucial factors that determine their sequential appearance under varied concentration, temperature, and solvent conditions. Particularly, the anticooperative nature is crucial for inducing the dominant appearance of H-aggregates at relatively low degrees of polymerization (aggregation), even though they are intrinsically disfavored by the thermodynamic energetics in the long run.

Based on these thermodynamic analyses, it is clear that tempering the stability of low oligomers along the anticooperative path could help eliminate the corresponding aggregate structures and thus simplify the assembly course and supramolecular structures. We then modify the structure of **1** by tweaking its steric feature of the molecule and raise the energy of low H-aggregates by intensifying steric hindrance. As expected, the H-aggregation pathway is successfully suppressed. That is, the new derivative **2** (Chart 1) only exhibits the J-aggregated state, which still presents a cooperative growth feature. This achievement clearly approves our analysis and understanding about the dependence of the supramolecular aggregation motif on chemical structure, and the conclusions drawn from there lend us with improved capability at controlling the supramolecular structure and properties.

RESULTS AND DISCUSSION

Aggregation Behaviors of 1. Previously, we showed that when a concentrated solution of **1** in $CHCl_3$ was dispersed in a large amount of aliphatic solvent (e.g., *n*-hexane or *n*-octane) J-aggregates were formed immediately, as evidenced by the appearance of a sharp and significantly red-shifted J-band around 900 nm (in comparison to the 0−0 peak of monomeric **1** at ca. 770 nm).[17] Then, a temperature-dependent study is carried out, and more complex behaviors are revealed. Specifically, when a solution of **1** in a binary solvent of $CHCl_3$/*n*-octane (8:92, v/v) is heated, the J-band is observed to subside continuously with increasing temperature until it disappears completely at about 320 K (Figure 2a). Such spectral changes not surprisingly correspond to the dissociation of J-aggregates at elevated temperatures. Interestingly, when the absorption coefficient changes of the J-band are plotted against temperature, the resultant curve clearly deviates from the behavior of an isodesmic system (Figure S2), by showing a relatively abrupt transition around 315 K (Figure 2a, inset). Such a nonsigmoidal curve typically indicates a cooperative

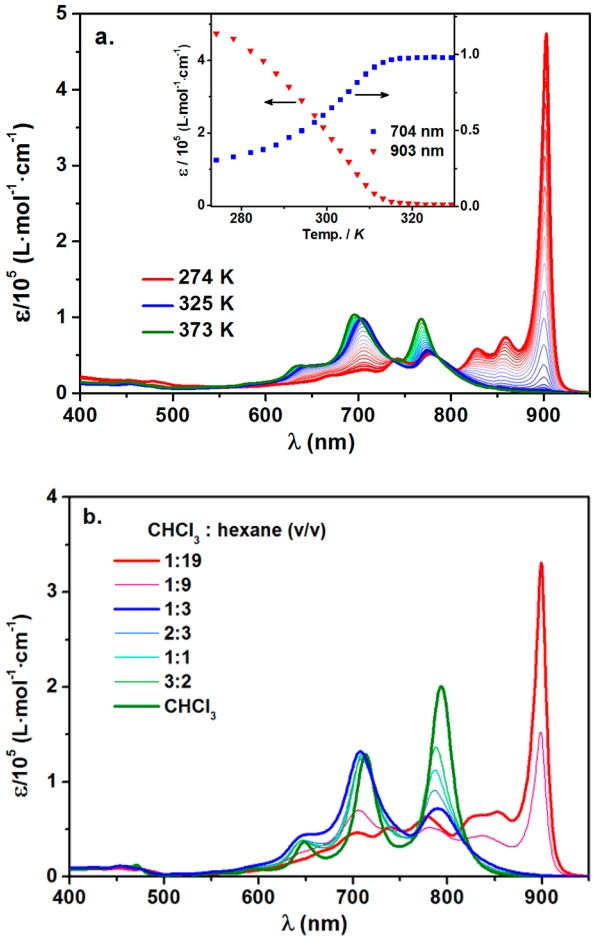

Figure 2. (a) Temperature-dependent absorption spectra of **1** (4.0×10^{-6} M) in $CHCl_3$/*n*-octane (8:92, v/v; the red and blue bold-lined spectra correspond to J- and H-aggregate-dominated states, respectively). Inset: absorption coefficient changes with temperature, unveiling the N−E assembly of J-aggregates. (b) Absorption spectra of **1** (1.0×10^{-5} M) in a series of mixed solvents (solvent content as indicated; red, blue, and green bold-lined spectra correspond to J-aggregate, H-aggregate, and monomer dominated states, respectively).

(i.e., N−E) assembly process (Figure S2).[14,17,18] Meanwhile, as the J-band diminishes from 275 to 320 K, the absorption peak at ca. 700 nm steadily gained its intensity, also showing a nonsigmoidal transition complementary to the change of J-band (Figure 2a, inset). This phenomenon corroborates the cooperative (N−E) assembling feature of the J-aggregate. An enthalpy change of about −43 kJ mol^{-1} is estimated for the elongation process of molecule **1**.[16a]

Nonetheless, some very unusual trends are observed with the peak intensity changes around 770 and 700 nm with continuously increased temperature (Figure S1). Specifically, in contrast to the significant attenuation of J-band and simultaneous rising of the peak at about 700 nm, the band around 770 nm remains nearly unchanged from 275 to about 310 K. Then, at above 310 K the 0−0 peak around 700 nm starts to grow substantially, but the 0−1 peak at about 770 nm exhibits minimal further changes in this higher-temperature range. As a result of such unconcerted intensity changes of 0−0 and 0−1 transitions, a series of absorption spectra with 0−1 peak higher than 0−0 peak emerge in the medium-temperature range, which is a prominent signature of H-aggregates.[6b] Hence, these observations strongly suggest that with increasing

DOI: 10.1021/jacs.8b01463
J. Am. Chem. Soc. 2018, 140, 5764−5773

temperature the J-aggregates are first transformed to H-aggregates, which dissociate at even higher temperature.

A similar J- to H-aggregate transition is also observed by changing the solvent polarity, that is, by gradually decreasing the ratio of *n*-hexane/$CHCl_3$ in the binary solvent (Figure 2b). Specifically, in solvents containing 5% or less of $CHCl_3$, molecule **1** clearly assumes the J-aggregated state, showing an evident J-band at ca. 900 nm (Figure 2b). Upon increasing the $CHCl_3$ content in the mixed solvent, the J-band gradually drops until it completely vanishes. Meanwhile, the peak at ca. 705 nm rises substantially until $CHCl_3$ reaches about 30%, at which point the overall absorption spectrum is unambiguously consistent with an H-aggregate dominated state (blue line, Figure 2b). Further increasing the ratio of $CHCl_3$ leads to the more evident growth of the 0−0 peak, while the intensity of the 0−1 peak shows almost no further change. In pure $CHCl_3$, an absorption spectrum corresponding to nonaggregated **1** is shown, indicating the dissociation of H-aggregates.

The above temperature- and solvent-dependent studies reveal that the J-aggregates are the thermodynamically more stable species when the supramolecular polymerization is driven to more completion, as lowering the solution temperature or increasing the nonpolar solvent ratio both induce the transformation from H- to J-aggregates. At this point, we are intrigued to find out why the H-aggregates, in spite of their thermodynamically less favored nature, are able to intercept the J-aggregation path and clearly manifested as competing species. Unfortunately, the ^{1}H NMR spectra are not helpful with analyzing the H- and J-aggregate structures (Figure S21).[20] Thus, additional absorption spectroscopy studies are conducted, with a focus on the concentration-dependent experiments, as they exclude all complications possibly introduced by varied temperature or solvent conditions.

A binary solvent of $CHCl_3$/*n*-hexane at 3:17 (v/v) is selected to conduct the concentration-dependent study first because such a mixture allows monitoring a more complete transition from the J- to H-aggregate with the absorption spectroscopy in a viable concentration range. In this solvent, molecule **1** at 40 μM is found to exist mainly as J-aggregates, with some H-aggregates present as minor components, as shown by the medium intensity of the peak around 700 nm (Figure 3a). Upon diluting the solution to 10 μM, the progressive loss of J-band and continued escalation of the peak around 700 nm are clearly observed, with multiple isosbestic points manifested. The salient change of the J-band (~900 nm) confirms the cooperative N−E feature of J-aggregate formation. This transformation between J- and H-aggregates is in good agreement to that observed in the temperature- and solvent-dependent experiments. Furthermore, by scrutinizing peak intensity changes around 700 and 780 nm with concentration, additional interesting behaviors are unveiled for the H-aggregates of **1**. Above 10 μM, the absorption intensity around 780 nm exhibited little change, whereas the intensity attenuation around 700 nm more sensitively reflects the H-aggregate dissociation in coordination to J-aggregate formation. However, in the lower concentration range of 0.5−10 μM, the 0−0 and 0−1 peaks both decrease with increasing concentration (Figure 3b), with all isosbestic points shown above 10 μM disappearing. Such spectral properties are ascribable to the growth of H-aggregates in the size. Nonetheless, additional information is unveiled when the extinction coefficient changes of 0−0 and 0−1 peaks are plotted against the concentration (Figure 3c). Between 1 and 10 μM, the 0−0 and 0−1 peaks

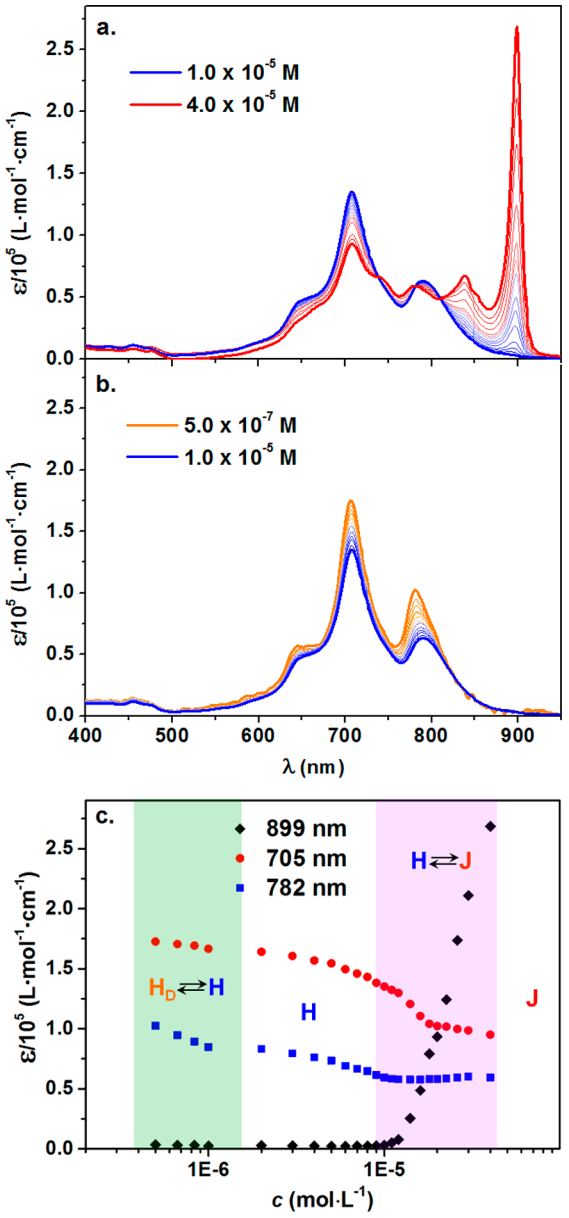

Figure 3. Concentration-dependent absorption spectra (a and b) of **1** in binary solvent of $CHCl_3$/*n*-hexane (3:17, v/v) at room temperature and (c) plots of extinction coefficients vs concentration. Colored regions show the approximate concentration ranges of major transitions among H-dimer ($\mathbf{H_D}$), higher H-aggregates (**H**), and J-aggregates (**J**).

show similar trends in their intensity change with concentration, and they nearly reach a plateau around 2 μM. However, when the concentration is further decreased from 1 to 0.5 μM, greater intensity changes are detected, and the 0−0 peak increases even more significantly than the 0−1 peak (Figure 3c). As the characteristic absorption feature of the H-aggregate (i.e., higher 0−1 than 0−0 peak) is consistently shown in a wide concentration range from 0.5 to 10 μM, the non-continuous peak intensity changes shown above and below 1 μM are attributed to transitions among different H-aggregated species.

In the above varied-concentration experiments, the absorbance of **1** at 0.5 μM is approaching the detection limit of the spectrophotometer, so further dissociation of H-aggregates at

DOI: 10.1021/jacs.8b01463
J. Am. Chem. Soc. 2018, 140, 5764−5773

even lower concentrations is not observable in that solvent ($CHCl_3$/*n*-hexane = 3:17, v/v). Based on the solvent-dependent study results, a mixed solvent of higher $CHCl_3$/*n*-hexane ratio (3:7, v/v) with weakened aromatic stacking interactions is employed to promote the H-aggregate dissociation at a higher concentration. At a low concentration of 0.17 μM, molecule **1** indeed exhibits an absorption band with a relatively low 0−1/0−0 ratio in more polar solvent (Figure 4a, green). By comparing this 0−1/0−0 ratio to that shown in pure chloroform (Figure 2b, green), it can be concluded that the binary solvent contains a mixture of monomeric **1** with some H-aggregated species. Upon increasing the concentration, the 0−0 peak decreases much more rapidly than the 0−1 peak, resulting in a continuously increased 0−1/0−0 ratio reflecting enhanced electronic coupling between aggregated molecules, thus potentially larger or more ordered H-aggregates. The H-aggregate spectral features persist to a very high concentration in this solvent, without the appearance of a J-band even at 0.3 mM. Very importantly, while the intensity of both 0−0 and 0−1 peaks shows a tendency to level off as the increasing concentration approached 0.1 mM, more dramatic intensity changes emerge at even higher concentration range of 0.1 to 0.3 mM. That is, a more pronounced extinction coefficient drop is exhibited by both the 0−0 and 0−1 peak at above 0.1 mM, which clearly deviates from the general trend demonstrated by the data points collected below 0.1 mM (Figure 4b). This phenomenon suggests the occurrence of new species at above 0.1 mM. Considering the much similar absorption band shape and 0−1/0−0 ratio, it is reasonable to correlate the transition shown above 0.1 mM in $CHCl_3$/*n*-hexane at 3:7 to that detected below 1 μM in $CHCl_3$/*n*-hexane at 3:17 (Figure 3c). Combining all the varied-concentration data collected from two binary solvent systems, we propose that the H-aggregation of **1** experienced two distinct stages. First, molecule **1** manifests a particularly stable H-type structure (most likely low H-oligomers) and then undergoes further transformation to (higher) H-aggregates. Though, at even higher concentration with suitable solvent polarity, the (high) H-aggregates can be transformed to J-aggregates.

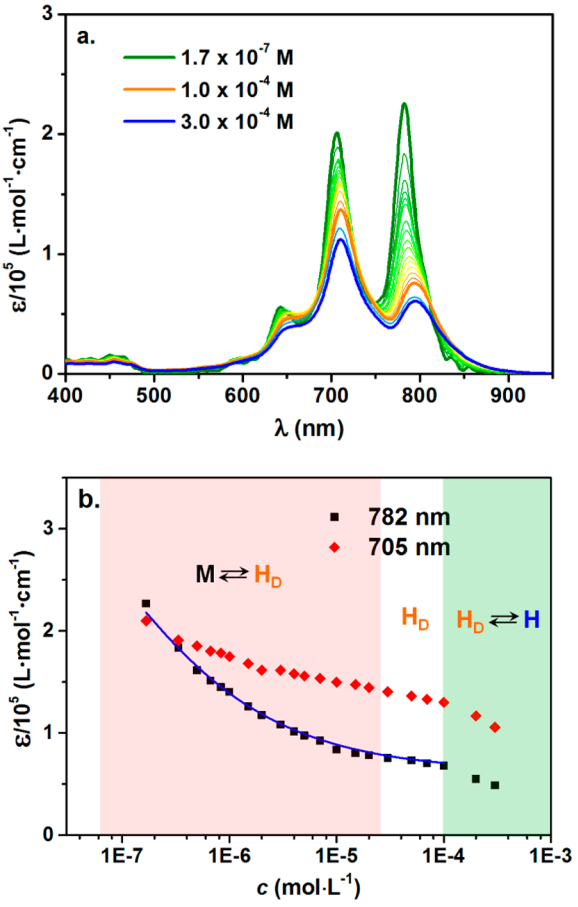

Figure 4. (a) Concentration-dependent absorption spectra of **1** in $CHCl_3$/*n*-hexane (3:7, v/v) at room temperature and (b) plots of extinction coefficients vs concentration, showing the transitions among monomer, H-dimer ($\mathbf{H_D}$), and higher H-aggregates (**H**), via a H-dimer-dominated intermediate stage (blue solid line representing the best fit to the monomer−dimer two-component model, with a dimerization constant of 6.9×10^6 M^{-1} and Gibbs free energy change of −39.0 kJ mol^{-1}).

Since the above-mentioned intermediate state shows absorption characteristics consistent with H-aggregates (i.e., large 0−1/0−0 ratio), we speculate it most likely involved some low oligomeric H-type species. Due to the nearest-neighbor electronic effect, it is reasonable for low oligomers to show more pronounced size-dependent spectral changes and thus discernibly different band shapes than higher aggregates.[14a,19] Theoretical simulations are conducted with an infinite self-association model featuring the dimerization constant varied from those associated with higher-aggregate formation (i.e., $K_2 \neq K$, see the SI for more details), and the calculation results demonstrate that a tight dimerization ($K_2 \gg K$) characteristic[15] can indeed entail the self-aggregation to show two distinct stages (Figure S11). That is, an intermediate state featuring the dominance of dimeric species can become clearly discernible, similar to that observed in our varied-concentration experiments. This result unambiguously corroborates our hypothesis that the complex H-aggregation behaviors exhibited by **1** are resultant from an anticooperative assembly mechanism involving highly stable low oligomers.

In order to experimentally prove that the absorption spectrum recorded from the intermediate stage in the concentration-dependency study could originate from certain low oligomers of H-aggregated **1**, a molecule that mimicked the dimer of **1** is designed and synthesized. In this molecule **1-D**, two polycyclic analogues of **1** are covalently connected through a long, flexible linker (Figure 5). As the intramolecular interaction is much more favored than intermolecular aggregation in dilute solution, a "folded" conformation of **1-D** (with two polycyclic subunits stacked intramolecularly; Scheme S1 in the SI) is expected under suitable conditions. The intermolecular stacking can be precluded at extremely low concentrations in polar solvents, such as chloroform. The absorption spectrum of **1-D** is then recorded at 3×10^{-7} M in $CHCl_3$, which is found to show very similar band shape to those collected from **1** at 0.1 mM and 0.5 μM in $CHCl_3$/*n*-hexane at 3:7 and 3:17 (v/v), respectively (Figure 5). The large 0−1/0−0 ratio proves that **1-D** was in the "folded" conformation under such conditions, with the two subunits adopting an intramolecular H-type stacking motif. The absence of intermolecular stacking is confirmed by the nearly concentration-independent band shape in the low concentration range (Figure S4). The minor wavelength variation among the three spectra is reasonably attributed to the solvent polarity difference and likely the replacement of Br by an alkylthio- group as well. The very similar band shapes to that of

DOI: 10.1021/jacs.8b01463
J. Am. Chem. Soc. 2018, 140, 5764−5773

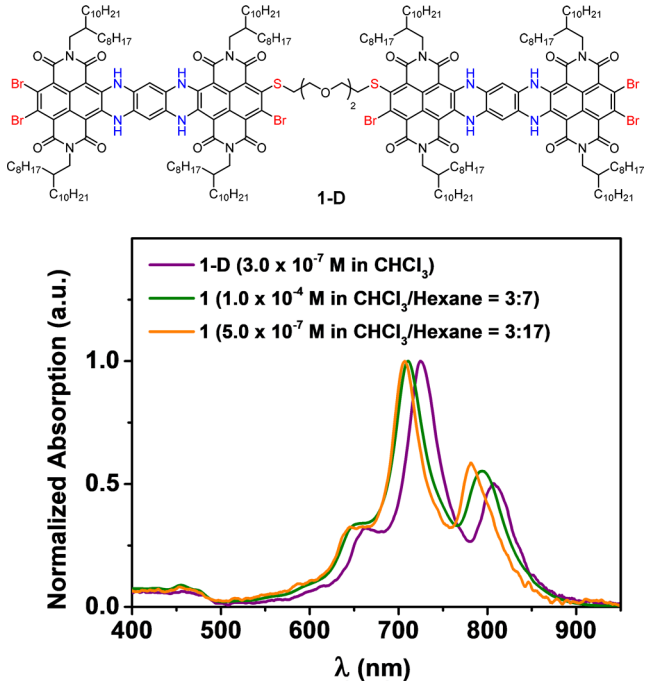

Figure 5. Structure of **1-D** and its absorption spectrum (purple) in comparison to those of **1** under the described conditions (binary solvent volume ratios of $CHCl_3$/*n*-hexane shown in parentheses).

1-D clearly indicate that the H-dimer ($\mathbf{H_D}$) is the dominant form of **1** under provided conditions in the two mixed solvents. This result further supports our previous conclusion that molecule **1** mainly forms an H-dimer in the lower concentration range in $CHCl_3$/*n*-hexane at 3:7 (v/v), and the concentration of $\mathbf{H_D}$ reaches its maximum around 0.1 mM, beyond which $\mathbf{H_D}$ starts to transform into higher H-aggregates (**H**), manifesting further decreases with 0−0 and 0−1 peaks (green regime in Figure 4b). In $CHCl_3$/*n*-hexane at 3:17 (v/v), a similar transition between $\mathbf{H_D}$ and **H** takes place, only at much lower concentrations (below 1 μM, green regime in Figure 3c). Moreover, **1-D** is found to maintain the "folded" conformation in pure chloroform even at elevated temperatures (Figure S4). This phenomenon substantiates the notion that $\mathbf{H_D}$ is particularly stable, which constitutes the basis for the anticooperative growth of H-aggregates.

Next, the molecular structural basis for the highly stable dimer $\mathbf{H_D}$ of **1** is analyzed. It is well documented by now that the molecules in H-aggregates necessarily assume a small lateral offset with respect to their transition dipoles.[4] Evidently, within such a stacking motif, the branched, bulky alkyl side chains installed around the polycyclic skeleton of **1** are placed very close to one another. In the dimer form, there is ample space on both sides of the stacked molecules to accommodate these alkyl chains (Figure 6).[14a,19] However, as the size of H-aggregates grows larger and larger, the void space available for each molecule diminishes, and steric congestion continuously builds up. It is thus reasonable to expect the thermodynamic driving force for aggregation to attenuate with increasing size of H-aggregates, giving rise to the anticooperative growth. An effective way to reduce the steric congestion among side chains is apparently to assume a greater offset along the long axis of the polycyclic skeleton, which happens to be the orientation of the transition dipole in **1** (Chart 1). Therefore, such a packing motif change may lead to a switch from H- to J-type exciton

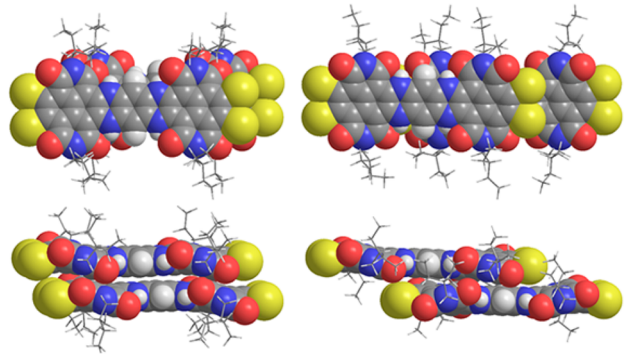

Figure 6. Top and side views of molecular arrangements in H- (left) and J- (right) dimers, calculated with energy minimization (MM2) (long alkyl chains were shortened in calculations).

coupling. Apparently, the J-aggregates experience less steric hindrance and thus higher thermodynamic stability, due to the spatially more segregated side chains (Figure 6) and most likely the laterally, instead of vertically, extended propagation motif (*vide infra*). Nonetheless, a smaller aromatic stacking surface is apparently possessed by a J-dimer, which could account for its lower stability and the cooperative feature of J-aggregation.

Taking advantage of the different solvent and concentration conditions promoting the H- and J-aggregate formations, we are able to obtain these aggregates separately and characterize their respective morphologies. AFM images are collected by drop-casting solutions of **1** that stabilized H- and J-aggregates, respectively. It is found that the J-aggregates form long, fibrous nanowires of several micrometers long and 2−3 nm high, whereas the H-aggregates are observed in the form nanoparticles with irregular sizes (Figures 7 and S6). Such disparate morphologies clearly reflect the dissimilar molecular packing motifs in H- and J-aggregates. The irregular nanoparticle morphology is consistent with our hypothesis about the influence of steric effects on the size of H-aggregates. The progressively built-up steric hindrance and anticooperative feature preclude H-aggregates from growing into larger sizes, and the smaller nanoparticles formed in solution likely amalgamate in a disordered fashion and convert to larger, irregular assemblies during solvent evaporation. In contrast, the fibril morphology reflects the ability of a J-aggregate to grow with a long-range order. The height dimension (2−3 nm) of the J-aggregate fibers revealed by AFM (Figure 7a) is comparable to the molecular size of **1** (Figure S6), suggesting "string"- or "brick"-type molecular packing motifs, which have been commonly observed for J-aggregates,[8] likely occurred to

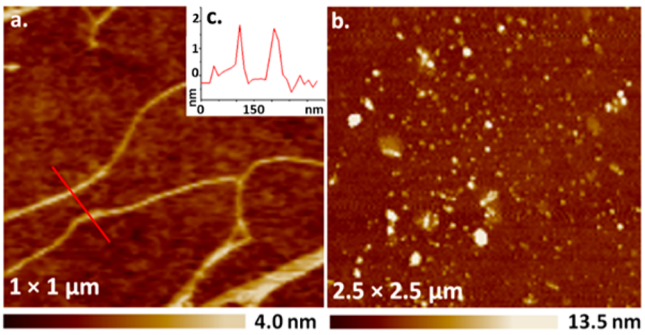

Figure 7. AFM (height) images of J- (a) and H- (b) aggregates of **1** and (c) the height profile along the red line in (a).

DOI: 10.1021/jacs.8b01463
J. Am. Chem. Soc. 2018, 140, 5764−5773

the fibers. Such laterally extended assembling structures are also agreeable to the cooperative growth feature.[9b,e,10g,16f] To summarize the above analyses, the H-aggregation path manifests a higher dimerization constant because of the larger intermolecular stacking surface areas, and thus some H-aggregate oligomers are able to grow preferentially until the steric hindrance becomes too severe. In contrast, the double-layered "string" or few-layered "brick" J-aggregates, in spite of their energy-disfavored oligomerization (nucleation) process, are void of continued accumulation of steric strain, for adopting the laterally extended packing motif, and are able to grow in the form of long dimensioned fibers. When a sufficient number of molecules are associated with greater energy gained, the J-aggregates are able to override the H-aggregates and appear to be the dominant species.

Modeling Analyses of Dual-Aggregation-Pathway Systems. In view of such interesting behaviors exhibited by two competing (cooperative and anticooperative) assembly paths, besides the above experimental-based analyses, a mathematic model is set up to quantitatively study and illustrate the inherent thermodynamic properties of such unique supramolecular systems.[10d,15] In our current model, four variants are introduced to describe the two different pathways, with K_2 and K_2' defined as the dimerization constants, while K and K' represent the association constants of stepwise monomer addition to form higher aggregates, respectively (Scheme 1). By defining $K_2 < K$ and $K_2' > K'$, the

Scheme 1. Schematic Representation of a Stepwise (Supramolecular) Polymerization System Comprising Two Competing Pathways

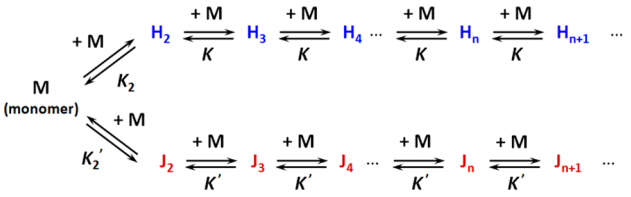

cooperative and anticooperative growth features are bestowed. We are fully aware that more sophisticated situations most likely occur to real systems, and a greater number of variants are required in order to accurately replicate them. However, using this simplified model with minimized calculations, the most important and representative properties can already be delineated.

Based on this model, the concentration of molecules forming aggregates H_n ($c_H = 2 \times [H_2] + 3 \times [H_3] + \ldots n \times [H_n] + \ldots$) via the anticooperative path can be expressed as (see the SI)

$$c_H = \frac{K_2[M]}{K}\left(\frac{1}{(1 - K[M])^2} - 1\right) \quad (K_2 > K, \text{ anticooperative}) \tag{1}$$

where [M] represents the concentration of molecules that remain in the monomeric state at equilibrium. Similarly, the concentration (c_J) of molecules composing aggregates J_n ($c_J = 2 \times [J_2] + 3 \times [J_3] + \ldots n \times [J_n] + \ldots$) along the cooperative path can be written as

$$c_J = \frac{K_2'[M]}{K'}\left(\frac{1}{(1 - K'[M])^2} - 1\right) \quad (K_2' < K', \text{ cooperative}) \tag{2}$$

The two aggregation paths are correlated by a given total concentration of molecules in the system

$$c_T = [M] + c_H + c_J \tag{3}$$

This bipath model (Scheme 1) conveniently accommodates the single-path situations. By setting $K_2' = K' = 0$ or $K_2 = K = 0$, the model is reduced to a single-path anticooperative or cooperative mechanism, respectively. Reasonably, the current model reproduces the previous results from analytic solutions.[11] Namely, as qualitatively illustrated in Figure 1, the most notable feature of single-path nonequal K polymerizations is that, given the same K and K' values, the cooperative and anticooperative systems afford higher and lower average degrees of polymerization than the isodesmic model, respectively (Figures S7–S9), evidencing the powerful impact of the dimerization constant (K_2 and K_2'). It is noteworthy that, in the case of an anticooperative system ($K_2 > K$ and $K_2' = K' = 0$), a particularly stable dimer can bring about a distinguishable two-step transition, corresponding to the monomer-to-dimer and dimer-to-higher aggregate stages (Figure S11). This phenomenon was observable in our experiments. Moreover, even though an isodesmic growth is defined beyond dimer formation, a pronounced even−odd effect is manifested (Figure S10).[14a] Namely, the species with an even-numbered degree of polymerization (dimer, tetramer, hexamer, and so on) are produced more abundantly than the odd-numbered (trimer, pentamer, heptmer, and so on).

Next, we set out to study the dual-path systems, particularly those boasting concurring cooperative and anticooperative mechanisms. A representative diagram qualitatively depicting the relative energy levels of different species, related to those observed in the aggregation of molecule **1**, is demonstrated in Figure 8a, and a set of distinctive behaviors are revealed (Figure 8b and SI). First of all, the existence of a competing (isodesmic or anticooperative) pathway "delays" the appearance of the cooperatively assembled aggregates (J_n in Scheme 1). That is, compared to a single-path system with the same K_2' and K', aggregates J_n are formed at higher concentrations when an anticooperative (or even isodesmic) aggregation path is present (Figures S13 and S14). The larger K_2, the higher concentration is required for J_n to appear and take over. Second, the anticooperatively formed aggregates (H_n's in Scheme 1) emerge as intermediate species at medium concentrations in the dual-path system, prior to the emergence of cooperatively assembled J_n's. The growths of H_n's are curtailed by the appearance of J_n's at higher molecular concentrations, provided that K' is larger than K (even if just very slightly). Accordingly, only low oligomers of H_n are observable (Figure S18). Moreover, when $K_2 \gg K$, H-dimer dominates in a certain concentration range prior to the presence of higher H- and J-aggregates (Figure 8b). In general, all these calculation results are in good agreement with the conclusions drawn from experimental data (*vide ante*). Furthermore, it is also shown that in the low concentration range the dual-path polymerization exhibits lower average degree of polymerization than an analogous single-path cooperative system with the same K_2' and K'. Nonetheless, at sufficiently high concentration, nearly identical degrees of polymerization are attained by the single- and dual-path

DOI: 10.1021/jacs.8b01463
J. Am. Chem. Soc. 2018, 140, 5764−5773

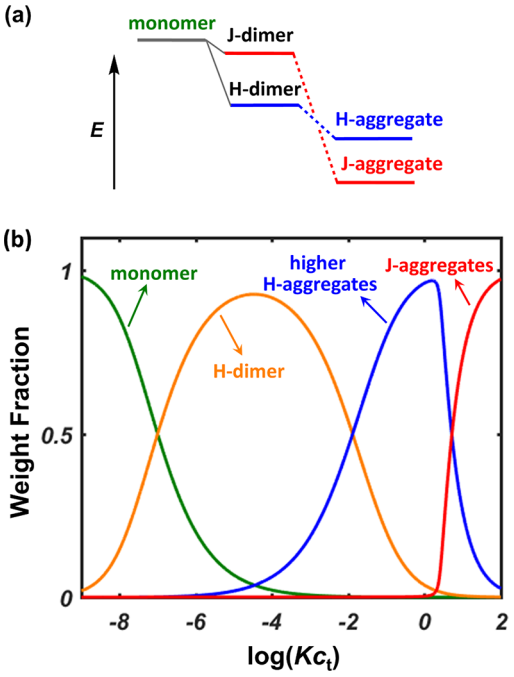

Figure 8. (a) Schematic qualitative representation of the relative energy levels of different species and (b) simulated weight fraction changes of monomer, H-dimer, higher H-aggregate, and J-aggregate as functions of Kc_T with representative association constants: $K_2/K = 1 \times 10^3$, $K_2'/K = 0.5$, and $K'/K = 1.1$.

systems (Figure S18), indicating that the competing path only alters the aggregate structure and distribution during the intermediate-conversion stage and that the eventual outcome is hardly affected if the polymerization can be driven to near completion.

It should be noted that the simulation results shown in Figure 8b and the SI are illustrated for representative dual-path systems with specific association constants applied. For a real molecular system exhibiting complex aggregation behaviors, such as **1**, it is practically difficult to precisely determine all the association constants and mapping out the species distributions by fitting the experimental data to the model (except for K_2 which can roughly be estimated; see the SI). One of the reasons is that simultaneous fitting of multiple variants (association constants) and unknowns (including extinction coefficients of all species) necessarily renders the fitting results less reliable. Moreover, as seen in Figure 8b, a complete transformation from monomer to fully aggregated state (J_n) typically spans a concentration range of ca. 10 orders of magnitude with given association constants. Thus, it is not viable to obtain a complete set of experimental data in a single solvent, due to the limited instrumentation detection range of a given characterization technique (e.g., absorption spectroscopy). In practice, a complete transformation is monitored by combining the data collected from a set of different solvents, each covering a certain concentration range (e.g., Figures 3 and 4). Then, the requirement for converting thermodynamic parameters in different solvents (see the SI) introduces additional errors. Furthermore, as mentioned above a real system possibly exhibits a series of gradually changed association constants, inevitably entailing deviations from the simple model introduced here comprising only four variants. Nonetheless, in spite of the higher complexity of real systems, the current simulation serves well in demonstrating the principal thermodynamic features brought by concurring cooperative and anticooperative assembly paths.

Single-Path J-Aggregation Design. Based on the above theoretical studies and experimental results, we are able to modulate the supramolecular behaviors through rational design and molecular modification. Since the J-aggregate is the ultimate predominant aggregate species at higher concentrations, it can be inferred that K is smaller than K' for **1**. It is clear from the theoretical analyses that the key factor that determined the appearance of H-aggregates was a large K_2 value. It should thus be possible to bypass the H-aggregate intermediates by tempering the stability of the H-dimer. By analyzing the molecular structure of **1**, we speculate that suitable steric hindrance and certain conformational flexibility of the side chains on **1** are likely of vital importance to the high stability of an H-dimer. This is because, although the alkyl side chains are placed very close to one another in a H-dimer, with a β-branching point they should be able to minimize the spatial congestion by rotating to specific orientations and occupying the ample empty space outside the dimer. However, in H-trimer and face-to-face stacked higher aggregates the space available to accommodate side chains on internal molecules became increasingly limited. Hence, $\mathbf{H_D}$ exhibits relatively small steric repulsion and thus higher stability.

Based on these analyses, we deem that if more rigid side groups are introduced to molecule **1** the steric repulsion among the side chains can be intensified in the H-dimer because the inflexible side groups would lack the ability to avoid each other even in the dimer state. Thereby, the H-dimer can be destabilized, and the H-aggregates may accordingly be suppressed or even eliminated.[21f] Subsequently, we design a new molecule **2**, which has the β-branched alkyl chains partially replaced by mesityl groups. Because the mesityl groups entailed not only lower flexibility but also much lower solubility, only two of the four side chains are replaced (Chart 1), as the remaining two long alkyl side chains are indispensable for retaining adequate molecular solubility in less polar solvents and allowing for suitable aggregation kinetics required by formation of ordered supramolecular structures. Indeed, as expected, the H-aggregate formation is frustrated, and only the J-aggregates are observable with molecule **2**, shown by the prominent J-band at 874 nm (Figure 9a). Importantly, during the gradual transformation from monomer to J-aggregate, no evidence for H-aggregate formation was detected from the absorption spectra, as proven by the constantly lower peak intensity at about 690 nm than 770 nm (Figures S5a and S12).[7b] The varied-temperature absorption spectra clearly show a pseudoisosbestic point (Figure 9a), which also supports a simple two-state (monomer to J-aggregate) transition, without an intermediate (H-aggregation) state. The J-band wavelength exhibited by **2** is slightly blue-shifted relative to that of **1**, suggesting that the lateral slipping angles, vertical stacking distances, and/or aggregate sizes are slightly differed for J-aggregates of **1** and **2**. This is not completely surprising, in consideration of the electronic and steric differences imposed by the side groups. The J-aggregation of **2** is also a cooperative process, as shown by the nonsigmoidal curves depicted by the extinction coefficient change with both temperature and concentration (Figures 9b and S12). The enthalpy change associated with the elongation process is estimated to be about -41 kJ mol^{-1}, comparable to that of molecule **1** (Figures S2 and S5). By fitting the concentration-dependent data from the $CHCl_3$/*n*-hexane (v/v = 17:83) solution to the single-path K_2–

DOI: 10.1021/jacs.8b01463
J. Am. Chem. Soc. 2018, 140, 5764−5773

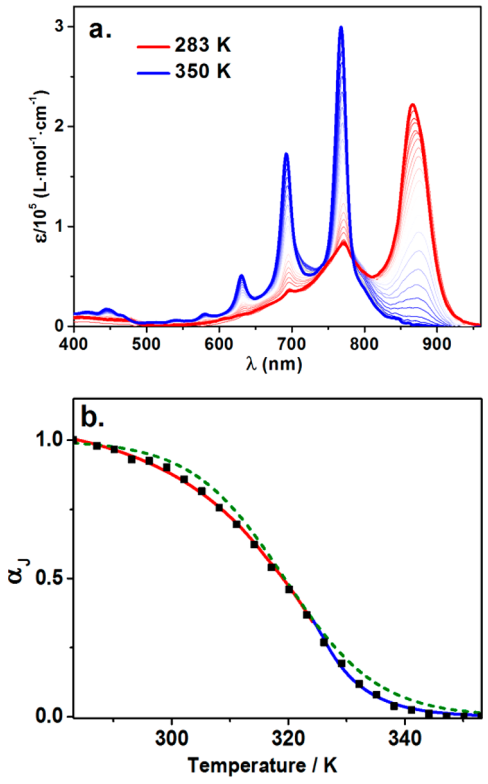

Figure 9. Temperature-dependent absorption spectra (a) of **2** in cyclohexane at 1.5×10^{-5} M and (b) fraction of J-aggregated **2** (α_J) as a function of temperature (estimated based on the extinction coefficient change at 874 nm), shown with the best fit to the (single-path) N–E model (red line, elongation regime; blue line, nucleation regime) in comparison to the isodesmic model (green dashed line).

K model, the corresponding association constants are estimated to be $K_2 = 1.1 \times 10^3$ and $K = 1.2 \times 10^6$ M^{-1} (Figure S12). The absence of H-aggregation with molecule **2** underlines the highly sensitive and subtle dependence of supramolecular structure on the molecular structure. The fact that the H-pathway is successfully suppressed by fine-tuning the steric property via side-group modification sheds important light on the design principles of J-aggregated supramolecular structures.

CONCLUSION

An N-heterocyclic aromatic dicarboximide molecule **1** is found to exhibit interesting dual-path self-aggregation behaviors. That is, the H- and J-aggregates appear sequentially in solution when suitable conditions are provided to promote a transition from lower to higher degrees of self-association. By carefully scrutinizing the temperature- and concentration-dependent absorption spectra, the J- and H-aggregates of **1** are proven to possess cooperative and anticooperative assembling mechanisms, respectively. By virtue of the distinctive optical properties of H- and J-aggregates, this unique supramolecular system lends special opportunities for an in-depth study on the complex self-aggregation behaviors featuring competing cooperative and anticooperative paths.

In order to better understand the thermodynamic basis of the sequential appearance of H- and J-aggregates with **1**, a mathematic model accommodating two concurring polymerization paths, both featuring nonisodesmic (K_2–K) growth characteristics, is set up for theoretically simulating the properties of such dual-path polymerization systems. The results in general very well explain the experimental observations, and a few important conclusions are revealed as follows. First, when two polymerization paths, one anticooperative ($K_2 > K$) and the other cooperative ($K_2' < K'$), are concurring and competing, the anticooperatively formed products (basically oligomers) arise first, under conditions that promote a low to medium degree of polymerization. Second, as long as K' is larger than K, even if just very slightly, the high polymers produced from the cooperative path would eventually take over at a higher degree of polymerization and become the predominant species when the polymerization (or self-association) equilibrium is pushed to near completion (Figure 8). Last but not the least, the calculation results also indicate that if K_2 in the anticooperative path is effectively reduced the competing path may be completely circumvented. Thus, by tweaking the chemical structure of molecule **1**, specifically by introducing more rigid and bulky aryl side chains, the steric property of the molecule is modified, and the stability of its dimer is presumably hampered. As expected, the H-aggregation path is successfully bypassed, as evidenced by molecule **2** which exhibits a single, cooperative self-assembly motif of J-aggregate. This achievement at modulating the supramolecular behaviors through rational design and chemical modification helps prove our understanding about the molecular structure basis of the supramolecular property in the current system, as well as our improved ability at controlling the supramolecular architectures.

ASSOCIATED CONTENT

Supporting Information

The Supporting Information is available free of charge on the ACS Publications website at DOI: 10.1021/jacs.8b01463.

Experimental procedures and analytical data (PDF)

AUTHOR INFORMATION

Corresponding Authors

*dhzhao@pku.edu.cn

*yanqifan@ecust.edu.cn

ORCID

Kang Cai: 0000-0002-8883-0142

Qifan Yan: 0000-0002-5784-5560

Dahui Zhao: 0000-0002-4983-4060

Author Contributions

§K. C. and J. X. contributed equally. The manuscript was written through contributions of all authors.

Notes

The authors declare no competing financial interest.

ACKNOWLEDGMENTS

The work is financially supported by the National Natural Science Foundation of China (Nos. 51473003, 21674001, and 21602061). We acknowledge the High-performance Computing Platform of Peking University for the computational resources.

REFERENCES

(1) (a) Kim, F. S.; Ren, G.; Jenekhe, S. A. *Chem. Mater.* **2011**, *23*, 682–732. (b) Aida, T.; Meijer, E. W.; Stupp, S. I. *Science* **2012**, *335*, 813–817. (c) Yan, Q.; Luo, Z.; Cai, K.; Ma, Y.; Zhao, D. *Chem. Soc. Rev.* **2014**, *43*, 4199–4221.

DOI: 10.1021/jacs.8b01463
J. Am. Chem. Soc. 2018, 140, 5764–5773

(2) (a) Varghese, S.; Das, S. *J. Phys. Chem. Lett.* **2011**, *2*, 863−873. (b) Wang, C.; Dong, H.; Hu, W.; Liu, Y.; Zhu, D. *Chem. Rev.* **2012**, *112*, 2208−2267. (c) Mei, J.; Diao, Y.; Appleton, A. L.; Fang, L.; Bao, Z. *J. Am. Chem. Soc.* **2013**, *135*, 6724−6746.
(3) (a) Dong, H.; Wang, C.; Hu, W. *Chem. Commun.* **2010**, *46*, 5211−5222. (b) Varghese, S.; Das, S. *J. Phys. Chem. Lett.* **2011**, *2*, 863−873. (c) Wang, L.; Olivier, Y.; Prezhdo, O. V.; Beljonne, D. *J. Phys. Chem. Lett.* **2014**, *5*, 3345−3353. (d) Dou, J. − H.; Zheng, Y. − Q.; Yao, Z. − F.; Yu, Z. − A.; Lei, L.; Shen, X.; Luo, X. Y.; Sun, J. − L.; Zhang, S. − D.; Ding, Y. − F.; Han, G.; Yi, Y.; Wang, J. − Y.; Pei, J. *J. Am. Chem. Soc.* **2015**, *137*, 15947−15956.
(4) (a) McRae, E. G.; Kasha, M. *J. Chem. Phys.* **1958**, *28*, 721−722. (b) Kasha, M.; Rawls, R.; El-Bayoumi, M. A. *Pure Appl. Chem.* **1965**, *11*, 371−392. (c) Siddiqui, S.; Spano, F. C. *Chem. Phys. Lett.* **1999**, *308*, 99−105. (d) Sung, J.; Kim, P.; Fimmel, B.; Würthner, F.; Kim, D. *Nat. Commun.* **2015**, *6*, 8646−8652.
(5) (a) He, T.; Stolte, M.; Burschka, C.; Hansen, N. H.; Musiol, D.; Kälblein, D.; Pflaum, J.; Tao, X.; Brill, J.; Würthner, F. *Nat. Commun.* **2014**, *6*, 5954−5962. (b) Dou, J.−H.; Zheng, Y. − Q.; Yao, Z. − F.; Yu, Z. − A.; Lei, T.; Shen, X.; Luo, X. − Y.; Sun, J. − L.; Zhang, S. − D.; Ding, Y.-F.; Han, G.; Yi, Y.; Wang, J. − Y.; Pei, J. *J. Am. Chem. Soc.* **2015**, *137*, 15947−15956. (c) Dou, J.-H.; Zheng, Y.-Q.; Yao, Z.-F.; Lei, T.; Luo, X. − Y.; Yu, Z.-A.; Zhang, S. − D.; Han, G.; Wang, Z.; Yi, Y.; Wang, J.-Y.; Jian, P. *Adv. Mater.* **2015**, *27*, 8051−8055.
(6) (a) Fofang, N. T.; Park, T.-H.; Neumann, O.; Mirin, N. A.; Nordlander, P.; Halas, N. J. *Nano Lett.* **2008**, *8*, 3481−3487. (b) Eisele, D. M.; Knoester, J.; Kirstein, S.; Rabe, J. P.; Vanden Bout, D. A. *Nat. Nanotechnol.* **2009**, *4*, 658−663. (c) Patil, A. J.; Lee, Y.-C.; Yang, J.-W.; Mann, S. *Angew. Chem.* **2012**, *124*, 757−761. (d) Saikin, S. K.; Eisfeld, A.; Valleau, S.; Aspuru-Guzik, A. *Nanophotonics* **2013**, *2*, 21−38. (e) Yamagata, H.; Spano, F. C. *J. Phys. Chem. Lett.* **2014**, *5*, 622−632. (f) Patalag, L. J.; Ho, P. L.; Jones, P. G.; Werz, D. B. *J. Am. Chem. Soc.* **2017**, *139*, 15104−15113.
(7) (a) Mobius, D. *Adv. Mater.* **1995**, *7*, 437−444. (b) Spano, F. C. *Acc. Chem. Res.* **2010**, *43*, 429−439. (c) Würthner, F.; Kaiser, T. E.; Möller, C. R. S. *Angew. Chem., Int. Ed.* **2011**, *50*, 3376−3410. (d) Pochas, C. M.; Kistler, K. A.; Yamagata, H.; Matsika, S.; Spano, F. C. *J. Am. Chem. Soc.* **2013**, *135*, 3056−3066. (e) Hestand, N. J.; Spano, F. C. *Acc. Chem. Res.* **2017**, *50*, 341−350.
(8) (a) Wang, J.; Kulago, A.; Browne, W. R.; Feringa, B. L. *J. Am. Chem. Soc.* **2010**, *132*, 4191−4196. (b) Zitzler-Kunkel, A.; Lenze, M. R.; Meerholz, K.; Würthner, F. *Chem. Sci.* **2013**, *4*, 2071−2075. (c) Haedler, A. T.; Kreger, K.; Issac, A.; Wittmann, B.; Kivala, M.; Hammer, N.; Köhler, J.; Schmidt, H.-W.; Hildner, R. *Nature* **2015**, *523*, 196−200.
(9) (a) Kaiser, T. E.; Wang, H.; Stepanenko, V.; Würthner, F. *Angew. Chem., Int. Ed.* **2007**, *46*, 5541−5544. (b) Kaiser, T. E.; Stepanenko, V.; Würthner, F. *J. Am. Chem. Soc.* **2009**, *131*, 6719−6732. (c) Chan, J. M.; Tischler, J. R.; Kooi, S. E.; Bulović, V.; Swager, T. M. *J. Am. Chem. Soc.* **2009**, *131*, 5659−5666. (d) Xie, Z.; Stepanenko, V.; Radacki, K.; Würthner, F. *Chem. - Eur. J.* **2012**, *18*, 7060−7070. (e) Sengupta, S.; Würthner, F. *Acc. Chem. Res.* **2013**, *46*, 2498−2512. (f) Kar, H.; Gehrig, D. W.; Laquai, F.; Ghosh, S. *Nanoscale* **2015**, *7*, 6729−6736. (g) Kar, H.; Gehrig, D. W.; Allampally, N. K.; Fernández, G.; Laquai, F.; Ghosh, S. *Chem. Sci.* **2016**, *7*, 1115−1120. (h) Kar, H.; Ghosh, S. *Chem. Commun.* **2016**, *52*, 8818−8821. (i) Kar, H.; Gehrig, D. W.; Allampally, N. K.; Fernández, G.; Laquai, F.; Ghosh, S. *Chem. Sci.* **2016**, *7*, 1115−1120. (j) Chen, Z.; Liu, Y.; Wagner, W.; Stepanenko, V.; Ren, X.; Ogi, S.; Würthner, F. *Angew. Chem., Int. Ed.* **2017**, *56*, 5729−5733.
(10) (a) Maiti, N. C.; Mazumdar, S.; Periasamy, N. *J. Phys. Chem. B* **1998**, *102*, 1528−1538. (b) Yagai, S.; Seki, T.; Karatsu, T.; Kitamura, A.; Würthner, F. *Angew. Chem., Int. Ed.* **2008**, *47*, 3367−3371. (c) Berlepsch, H.; Böttcher, C. *J. Photochem. Photobiol., A* **2010**, *214*, 16−21. (d) Fennel, F.; Wolter, S.; Xie, Z.; Plötz, P. A.; Kühn, O.; Würthner, F.; Lochbrunner, S. *J. Am. Chem. Soc.* **2013**, *135*, 18722−18725. (e) Ogi, S.; Sugiyasu, K.; Manna, S.; Samitsu, S.; Takeuchi, M. *Nat. Chem.* **2014**, *6*, 188−195. (f) Yan, Q.; Cai, K.; Zhao, D. *Phys. Chem. Chem. Phys.* **2016**, *18*, 1905−1910. (g) Fukui, T.; Kawai, S.; Fujinuma, S.; Matsushita, Y.; Yasuda, T.; Sakurai, T.; Seki, S.; Takeuchi, M.; Sugiyasu, K. *Nat. Chem.* **2017**, *9*, 493−499.
(11) (a) Zhao, D.; Moore, J. S. *Org. Biomol. Chem.* **2003**, *1*, 3471−3491. (b) De Greef, T. F. A.; Smulders, M. M. J.; Wolffs, M.; Schenning, A. P. H. J.; Sijbesma, R. P.; Meijer, E. W. *Chem. Rev.* **2009**, *109*, 5687−5754.
(12) (a) Martin, R. B. *Chem. Rev.* **1996**, *96*, 3043−3064. (b) Chen, Z.; Lohr, A.; Saha-Möller, C. R.; Würthner, F. *Chem. Soc. Rev.* **2009**, *38*, 564−584. (c) Smulders, M. M. J.; Nieuwenhuizen, M. M. L.; de Greef, T. F. A.; van der Schoot, P.; Schenning, A. P. H. J.; Meijer, E. W. *Chem. - Eur. J.* **2010**, *16*, 362−367.
(13) (a) Zhao, D.; Yue, K. *Macromolecules* **2008**, *41*, 4029−4036. (b) Rest, C.; Kandanelli, A.; Fernández, G. *Chem. Soc. Rev.* **2015**, *44*, 2543−2572.
(14) (a) Gershberg, J.; Fennel, F.; Rehm, T. H.; Lochbrunner, S.; Würthner, F. *Chem. Sci.* **2016**, *7*, 1729−1737. (b) Baumgartner, R.; Fu, H.; Song, Z.; Lin, Y.; Cheng, J. *Nat. Chem.* **2017**, *9*, 614−622.
(15) (a) Zhao, D.; Moore, J. S. *J. Am. Chem. Soc.* **2003**, *125*, 16294−16299. (b) Zhao, D.; Moore, J. S. *Macromolecules* **2003**, *36*, 2712−2720.
(16) (a) Smulders, M. M. J.; Schenning, A. P. H. J.; Meijer, E. W. *J. Am. Chem. Soc.* **2008**, *130*, 606−611. (b) Markvoort, A. J.; ten Eikelder, H. M. M.; Hilbers, P. A. J.; de Greef, T. F. A.; Meijer, E. W. *Nat. Commun.* **2011**, *2*, 509. (c) Mayoral, M. J.; Rest, C.; Schellheimer, J.; Stepanenko, V.; Fernández, G. *Chem. - Eur. J.* **2012**, *18*, 15607−15611. (d) Mayoral, M. J.; Rest, C.; Stepanenko, V.; Schellheimer, J.; Albuquerque, R. Q.; Fernández, G. *J. Am. Chem. Soc.* **2013**, *135*, 2148−2151. (e) Kulkarni, C.; Bejagam, K. K.; Senanayak, S. P.; Narayan, K. S.; Balasubramanian, S.; George, S. J. *J. Am. Chem. Soc.* **2015**, *137*, 3924−3932. (f) van der Weegen, R.; Teunissen, A. J. P.; Meijer, E. W. *Chem. - Eur. J.* **2017**, *23*, 3773−3783.
(17) Cai, K.; Xie, J.; Zhao, D. *J. Am. Chem. Soc.* **2014**, *136*, 28−31.
(18) (a) Markvoort, A. J.; ten Eikelder, H. M. M.; Hilbers, P. A. J.; de Greef, T. F. A.; Meijer, E. W. *Nat. Commun.* **2011**, *2*, 509. (b) Korevaar, P. A.; George, S. J.; Markvoort, A. J.; Smulders, M. M. J.; Hilbers, P. A. J.; Schenning, A. P. H. J.; Greef, T. F. A. D.; Meijer, E. W. *Nature* **2012**, *481*, 492−496.
(19) Shao, Z.; Grüne, M.; Stolte, M.; Würthner, F. *Chem. - Eur. J.* **2012**, *18*, 13665−13677.
(20) Wu, J.; Fechtenkötter, A.; Gauss, J.; Watson, M. D.; Kasler, M.; Fechtenkötter, C.; Wagner, M.; Müllen, K. *J. Am. Chem. Soc.* **2004**, *126*, 11311−11321.
(21) For recent examples: (a) Ogi, S.; Grzeszkiewicz, C.; Würthner, F. *Chem. Sci.* **2018**, *9*, 2768−2773. (b) Ogi, S.; Matsumoto, K.; Yamaguchi, S. *Angew. Chem., Int. Ed.* **2018**, *57*, 2339−2343. (c) Chen, Z.; Liu, Y.; Wagner, W.; Stepanenko, V.; Ren, X.; Ogi, S.; Würthner, F. *Angew. Chem., Int. Ed.* **2017**, *56*, 5729−5733. (d) Wagner, W.; Wehner, M.; Stepanenko, V.; Ogi, S.; Würthner, F. *Angew. Chem., Int. Ed.* **2017**, *56*, 16008−16012. (e) Endo, M.; Fukui, T.; Jung, S. H.; Yagai, S.; Takeuchi, M.; Sugiyasu, K. *J. Am. Chem. Soc.* **2016**, *138*, 14347−14353. (f) Ogi, S.; Fukui, T.; Jue, M. J.; Takeuchi, M.; Sugiyasu, K. *Angew. Chem., Int. Ed.* **2014**, *53*, 14363−14367.

DOI: 10.1021/jacs.8b01463
J. Am. Chem. Soc. 2018, 140, 5764−5773